



Improved microwave absorption of Co-P/pollen composites synthesized by electroless plating

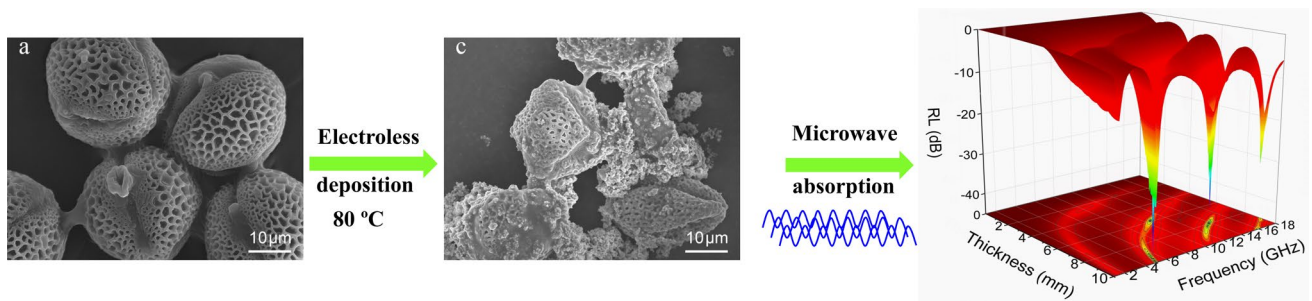
Jinxun Han¹ · Longfei Li¹ · Junsheng Xue¹ · Shenghui Zhang¹ · Hanzhuo Zhang¹

Received: 9 November 2020 / Accepted: 20 April 2021 / Published online: 24 May 2021
© The Author(s), under exclusive licence to Springer Nature B.V. 2021

Abstract

In this paper, electroless plating technologies were employed to prepare Co-P coatings on carbonized rape pollen as microwave absorption materials. Experimental results indicated microporous structures of rape pollen after a series of pretreatments, while uniform Co-P nanoparticles with diameters around 90 nm were deposited smoothly as coatings on and inside the irregular pollen walls. The Co-P/pollen composites exhibited a typical ferromagnetic characteristic with saturation magnetization of 32.6 emu g^{-1} and coercivity of 125.1 Oe. In microwave absorption analysis, dielectric loss was revealed with predominant effects than magnetic loss in frequency ranges of 5.0–8.2 GHz. A minimum reflection loss of -45.1 dB at 5.3 GHz was obtained with an increasing microwave absorption bandwidth up to 4.3 GHz.

Graphic abstract



Keywords Electroless plating · Cobalt-based alloys · Electromagnetic properties · Microwave absorption

1 Introduction

With the explosive development in electronic techniques, electromagnetic pollution has become a serious problem in everyday life, which damages human health and interferes electronic instrument operations [1–4]. To overcome this problem, great efforts have been made in recent decades to explore microwave absorption materials. According to electromagnetic attenuation mechanisms, microwave absorption

materials can be categorized into two types: magnetic loss materials (ferrites, magnetic metals, and intermetallics) and dielectric loss materials (carbonaceous materials, conductive polymers, and dielectric ceramics) [2]. Both two types of materials have certain defects and restrict their practical applications. Ferrites and magnetic metals, despite being the most commonly used, suffer from serious problems of being heavy, corrosive, and nondurable [3]. The drawbacks of carbonaceous materials and conductive polymers lie in costly and complicated synthesis processes as well as their disappointed high-temperature stability [4]. To date, materials in single phase cannot meet the severe demanding of microwave absorption. An efficient way is to fabricate composites based on magnetic/dielectric loss materials, which may possess the merit of synergistic effects on microwave

✉ Hanzhuo Zhang
zhz@cumt.edu.cn

¹ School of Materials and Physics, China University of Mining and Technology, Xuzhou 221116, People's Republic of China

energy dissipation. Examples have included NiFe₂O₄/RGO [5], carbon fiber/magnetic particles [6], and polyaniline/NiZn ferrites [7].

Electroless plating is prevalent in surface engineering with many advantages, such as low cost, simple equipment, preeminent environment stability and without substrate selection [8–10]. Furthermore, any part of the substrate can be coated as long as it is in contact with the plating solution, implying that the inner walls or holes of the components can be coated evenly. Electroless plating has been widely applied in the fields of wear resistance, anti-corrosion, and decoration. In recent years, it was used to prepare novel microwave absorbing composites. For example, Yang et al. coated Ni-Co-Fe-P on flake graphite with a minimum reflection loss of –12 dB at the frequency of 4.6 GHz when the absorber thickness was controlled around 3 mm [9]. Another research on electroless-plated Ni-Co-P/SiC composites revealed a broad effective microwave absorption band of 2.3 GHz [10]. Mechanisms for the improved performance of microwave absorbing composites which prepared by electroless plating have been fully discussed. Nevertheless, the microwave absorption capacity of the electroless-plated composites is not only dependent on their compositions but also related to their structures. In order to acquire high microwave absorbency, the structure of materials needs to be properly designed.

Rape pollen is a kind of carbonaceous organism with porous structures, which makes it a potential substrate to fabricate microwave absorption composites [11]. The porous structures of rape pollen contribute to prepare lightweight absorbers and trigger multiple reflections that may increase the transmission path of incoming electromagnetic waves, thus, improving the microwave attenuation ability [12, 13]. Therefore, excellent microwave absorbent can be anticipated if rape pollen is coated with magnetic metals or alloys. In this work, rape pollen powders were pretreated and electroless plated with quantities of Co-P nanoparticles that formed as uniform coatings. Their microstructures were characterized with the emphasis on the related microwave absorption performance.

2 Experimental methods

Rape pollen powders were purchased from Changbai Mountain Co., Ltd. Other chemicals were of analytical grade and applied without purification. Before electroless plating, a series of pretreatments on rape pollen powders were necessary. In a typical process, rape pollen powders were firstly immersed into glacial acetic acid for 5 min to destroy cell walls and to uncover their microporous structures. Then they were sensitized into an aqueous solution containing 12 g L⁻¹ SnCl₂·2H₂O and 35 mL L⁻¹ HCl for 5 min. After

washing with deionized water for several times, the pretreated rape pollen was activated in 10 mL L⁻¹ HCl solution with 0.5 g L⁻¹ PdCl₂ for 10 min. The electrolyte for electroless plating is composed of 24 g L⁻¹ CoSO₄·7H₂O, 68 g L⁻¹ Na₃C₆H₅O₇·2H₂O, 42 g L⁻¹ (NH₄)₂SO₄, and 28 g L⁻¹ NaH₂PO₂·H₂O. The pH value was adjusted to 10.5 by dilute NaOH solution, and the temperature was maintained at 80 °C. Combined with ultrasonic vibration, the pretreated rape pollen was poured into the electrolyte for 20 min. Then the coated rape pollen was rinsed three times with deionized water, dried at 80 °C in vacuum, and sintered at 200 °C under the atmosphere of Ar for 1 h.

Crystalline structures and surface morphologies of rape pollen before and after electroless plating were determined by X-ray diffraction (XRD Bruker D8 Advance) and scanning electron microscope (SEM FEI Quanta250), respectively. The composition was investigated via energy dispersive spectroscopy (EDS Bruker XFlash6). Thermogravimetry analysis (TGA) was conducted on high-temperature simultaneous thermal analyzer (STA NETZSCH 409PC) in the range of 20–1000 °C at a heating rate of 20 K/min under flowing Ar. The ASAP2020 Plus HD88 surface area analyzer was used for N₂ adsorption–desorption measurements and the specific surface area was calculated by using Brunauer–Emmett–Teller (BET) model. Hysteresis loop was tested through vibrating sample magnetometer (VSM Lakeshore 7407) with a magnetic field up to 2.0 T. By evenly mixed with paraffin wax at a ratio of 3:2 to obtain toroidal-shaped samples with an outer diameter of 7.0 mm and an inner diameter of 3.0 mm, the coated rape pollen was surveyed in a vector network analyzer (VNA Agilent HP8722ES) with the frequency range of 1.0–18.0 GHz to investigate its electromagnetic parameters.

3 Results and discussion

3.1 Characterization

Figure 1 compares XRD patterns of the rape pollen before and after electroless plating. For the primitive rape pollen, a broad diffuse peak is seen around 20 degree, which proves its carbonaceous organism in amorphous. By contrast, new diffraction peaks can be found in Co-P/pollen composites at $2\theta = 41.6^\circ$, 44.7° , and 47.6° , corresponding to (100), (002), and (101) crystal planes of ϵ -Co (JCPDS: 05-0727). Due to the solid solution of phosphorus in the lattice of cobalt, the diffraction peaks are right shifted in contrast to the standard Co patterns. Moreover, the relatively wide diffraction peaks indicate that the coated Co-P is in the nanoscale.

SEM images of the primitive rape pollen and Co-P/pollen composites are displayed in Fig. 2. It can be seen that the primitive rape pollen is nearly spherical with the average

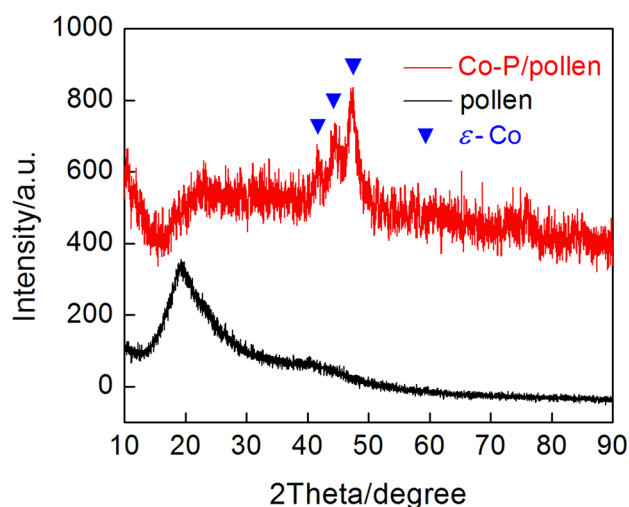


Fig. 1 XRD patterns of primitive rape pollen and Co-P/pollen composites

diameter around 20.1 μm . Irregular microholes are prevalent on their surfaces, and the walls between the microholes are curved with thicknesses around 350 nm. After electroless plating, numerous nanoparticles with diameters around 90 nm are deposited uniformly and formed as coatings on the surfaces of rape pollen. Protrusions can be observed on plated layers due to the aggregation and growth of Co-P nanoparticles [14]. At higher magnification, the walls between microholes of rape pollen become rougher after electroless plating. Furthermore, the interior of microholes is occupied by numerous Co-P nanoparticles, suggesting that the rape pollen is fully activated and plated. EDS mapping images shown in Fig. 2e confirm the existence of Co, P, O, and C elements, which are uniformly distributed in the Co-P/pollen composites with the compositions of 8.39 at%, 1.01 at%, 22.22 at%, and 68.37 at%, respectively. Combined with XRD and SEM analysis, it can be confirmed that the rape pollen has been successfully coated with Co-P nanoparticles in single-phase and hexagonal close-packed crystal structure.

Thermal stability of both primitive rape pollen and Co-P/pollen composites was examined by TGA measurements under Ar atmosphere and shown in Fig. 3. A slight weight loss of pollen and Co-P/pollen composites can be observed around 163 $^{\circ}\text{C}$, which is attributed to hydrogen bond rupture resulting in evaporation of water and other volatile components [15]. For primitive rape pollen, 33.7% weight loss in the range of 200–320 $^{\circ}\text{C}$ and 41.5% weight loss around 320–510 $^{\circ}\text{C}$ are mainly ascribed to the decomposition of intine and exine of pollen, respectively [16]. At higher temperature, weight loss is restrained since carbonization has been almost completed with adequate reactions among carbon, hydrogen, and oxygen. Due to the electroless-plated Co-P coatings on pollen surfaces, Co-P/pollen composites

show a much slower weight loss process than primitive rape pollen in the same temperature realm. From 500 to 900 $^{\circ}\text{C}$, weight loss of Co-P/pollen composites is decreased gradually from 47.3 to 20.7%. The phosphorus which is solidly dissolved in cobalt would form as Co_2P and/or CoP_2 during this temperature increasing process, and the out layer of electroless coatings might capture oxygen to form Co_3O_4 and/or CoO [15]. At 1000 $^{\circ}\text{C}$, the mass of pollen and composite material is still 4.5% and 18.6%, respectively; thus the content of Co-P can be calculated to be 14.1%.

In order to further investigate the specific surface area and pore structure, N_2 absorption–desorption tests were carried out on both primitive rape pollen and Co-P/pollen composites. As seen in Fig. 4, primitive rape pollen exhibits type III isotherm with low quantities of adsorption and negligible hysteresis loop, mainly because the cell walls are covered compactly on the pollen surfaces. Differently, Co-P/pollen composites have a typical Type IV isotherm with obvious hysteresis loop, indicating the presence of mesoporous structures. Compared with primitive rape pollen, specific surface area and total pore volume of Co-P/pollen composites increase from 11.4 $\text{m}^2 \text{g}^{-1}$ and 0.0195 $\text{cm}^3 \text{g}^{-1}$ to 18.6 $\text{m}^2 \text{g}^{-1}$ and 0.0689 $\text{cm}^3 \text{g}^{-1}$, respectively. The insets of Fig. 4a and b present pore size distributions of primitive rape pollen and Co-P/pollen composites which are in relative narrow ranges, while the pore size of primitive rape pollen corresponds to a higher pore volume. By carbonization and electroless plating, these porous structures can cause scattering absorption and multiple reflections, which are beneficial to enhance the microwave absorption performance [17].

3.2 Electromagnetic properties

The magnetic hysteresis loop of Co-P/pollen composites is presented in Fig. 5. A typical ferromagnetic characteristic can be confirmed, where the saturation magnetization (M_s) and coercivity (H_c) are 32.6 emu g^{-1} and 125.1 Oe, respectively. Magnetic properties of the composites should be derived from the Co-P nanoparticles. M_s of Co-P/pollen composites is much lower than that of the bulk Co (164.8 emu g^{-1}), resulting from the nano-sized Co-P particles and the existence of non-magnetic rape pollen [18]. Furthermore, the poor crystallinity of coated Co-P nanoparticles induces the increase of spin disorders and impairs the saturation magnetization [3, 19]. The value of H_c is known to be strongly dependent on phosphorus contents, crystal structures as well as lattice defects [5, 9, 20]. In the present study, H_c of the Co-P/pollen composites is similar to that of electroless-plated Co-P/Carbon Nanotubes [21], but much smaller than that of the Co-P/kaolin composites [22].

Complex permittivity ($\epsilon_r = \epsilon' - j\epsilon''$) and complex permeability ($\mu_r = \mu' - j\mu''$) of the Co-P/pollen composites as a function of frequency dependence are shown in Fig. 6. At

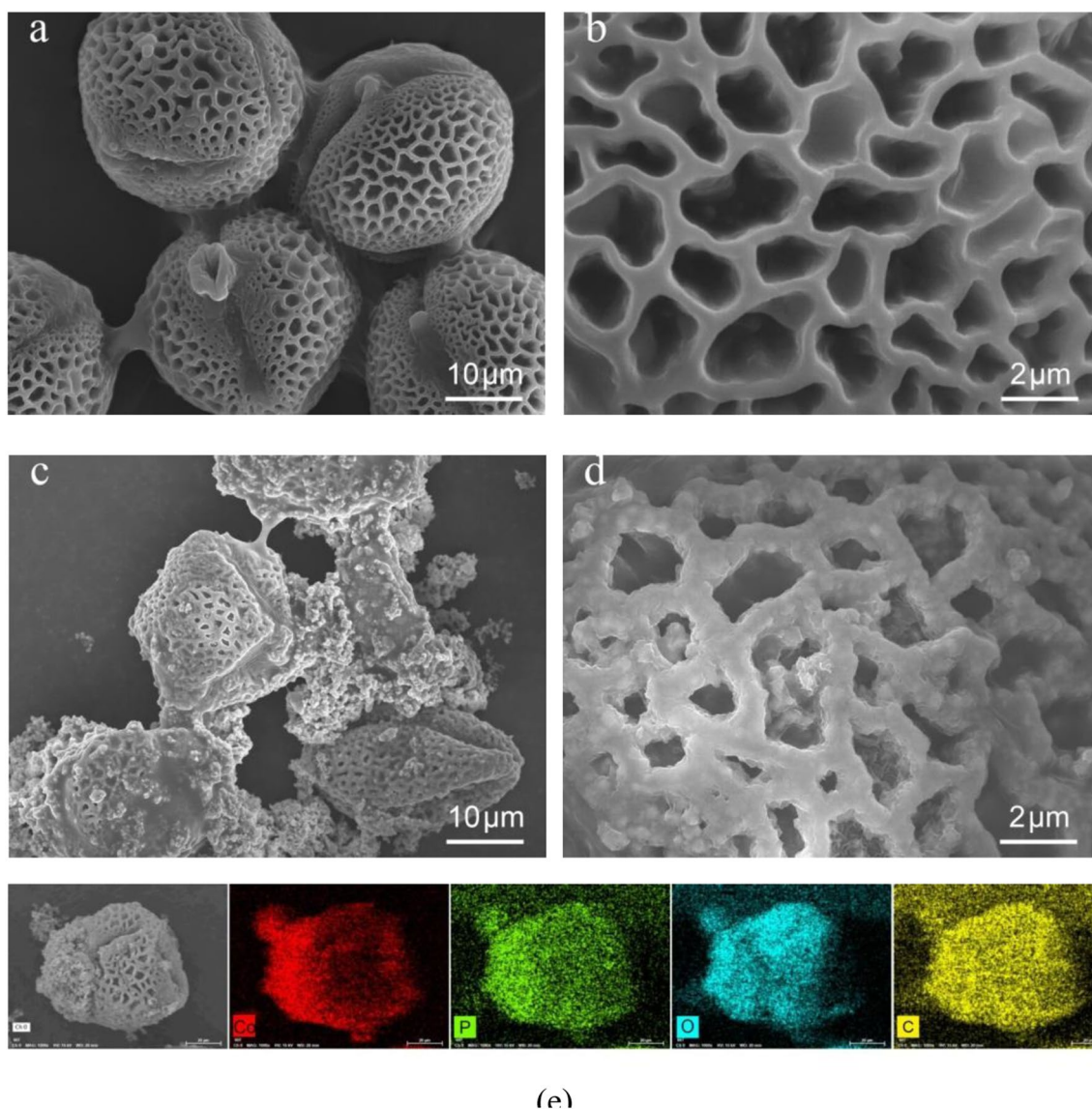


Fig. 2 SEM images of pretreated rape pollen (**a, b**) and Co-P/pollen composites (**c, d**), together with EDS mapping images of Co-P/pollen composites (**e**)

the tested frequency range, ϵ' varies in the range of 13.5 to 5.5, while ϵ'' decreases from 3.2 to 0.1. Higher ϵ' values at lower frequency are related with frequency dispersion effects caused by the increased lagging of polarization [7, 23]. The values of ϵ'' are larger than 1.3 in the range of 1.0–10.5 GHz, indicating an enhanced dielectric loss. As shown in Fig. 6b, μ' is relatively large and fluctuates around 2.0, while the values of μ'' vary between 0.2 and 0.13. A magnetic resonance peak occurs at 5.1 GHz in the curve of μ'' , which is favorable for improving the microwave absorption [24]. Figure 7 displays the dielectric loss tangent ($\tan\delta_\epsilon$) and magnetic loss tangent ($\tan\delta_\mu$) of the Co-P/pollen composites. It is observed that $\tan\delta_\epsilon$ fluctuates greatly between 0.24 and 0.02, while $\tan\delta_\mu$ varies within a narrow range around 0.1. The values

of $\tan\delta_\epsilon$ at 1.1–4.1 GHz and 5.8–12.4 GHz are greater than $\tan\delta_\mu$, suggesting that dielectric loss plays a more important role in microwave attenuation within these frequency ranges.

The mechanism of dielectric loss can be analyzed by Debye relaxation theory expressed as follows:

$$\left(\epsilon' - \frac{\epsilon_s + \epsilon_\infty}{2}\right)^2 + (\epsilon'')^2 = \left(\frac{\epsilon_s - \epsilon_\infty}{2}\right)^2, \quad (1)$$

where ϵ_∞ and ϵ_s are relative and static permittivity in infinite frequencies, respectively. The curves of ϵ' versus ϵ'' (known as Cole–Cole curves) would be a series of semicircles theoretically if the dielectric loss process is controlled only by Debye relaxation, and each semicircle represents a relaxation

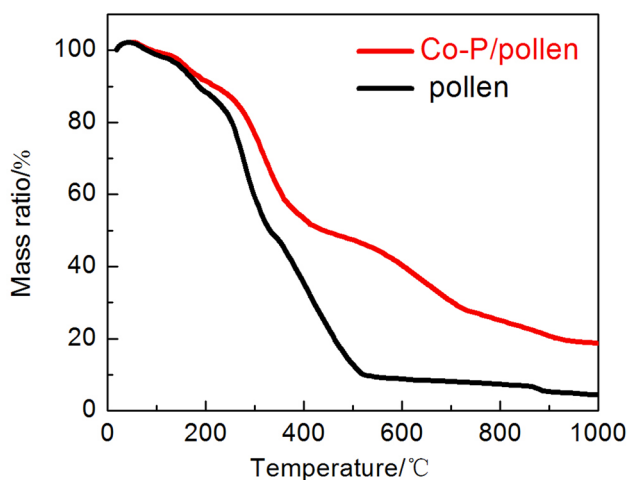


Fig. 3 TGA curves of pollen and Co-P/pollen composites

polarization behavior [3, 24]. For Co-P/pollen composites, a distorted curve with several semicircles are displayed in the range of 6.2–10.0 GHz in Fig. 8a, suggesting that the dielectric relaxation is combined with other polarization mechanisms. As is well known, dielectric loss can be derived from dipolar polarization, interfacial polarization, and conductivity loss in the range of 1.0–18.0 GHz [25]. The dipoles produced by defects and functional groups in Co-P/pollen composites could give rise to oriented polarization under alternating electromagnetic fields [26]. Besides, abundant heterogeneous interfaces between pollen and Co-P nanoparticles accumulate inhomogeneous space charge distributions, and thus, increase the interfacial polarization. Cole–cole curve exhibits as a straight line in the ϵ' range of 11.0–13.5, which implies that the dielectric loss is dominated by conductivity loss of Co-P nanoparticles and carbonized rape pollen [13, 27].

In general, magnetic loss initiates from various types of mechanisms including eddy-current loss, nature, and

exchange resonance in the range of 1.0–18.0 GHz [12, 28]. The contribution of eddy-current loss to magnetic loss can be analyzed by the following equation: $C_0 = \mu''(\mu')^{-2}f^{-1} = 2\pi \mu_0 d^2 \sigma / 3$, where f , μ_0 , d , and σ represents applied frequency, vacuum permeability, absorbent thickness, and electric conductivity, respectively. If the magnetic loss arises from eddy-current loss exclusively, the value of C_0 would be constant with the change of frequency. As shown in Fig. 8b, C_0 values of Co-P/pollen composites vary by the increment of frequency, suggesting that the magnetic loss is originated from the combined interactions of eddy-current effects with other loss mechanisms [29]. When the frequency exceeds 16.2 GHz, the constant value of C_0 suggests that the magnetic loss is reined by eddy-current loss. To interpret the microwave loss mechanisms of Co-P/pollen composites, attenuation constant is calculated according to the following equation:

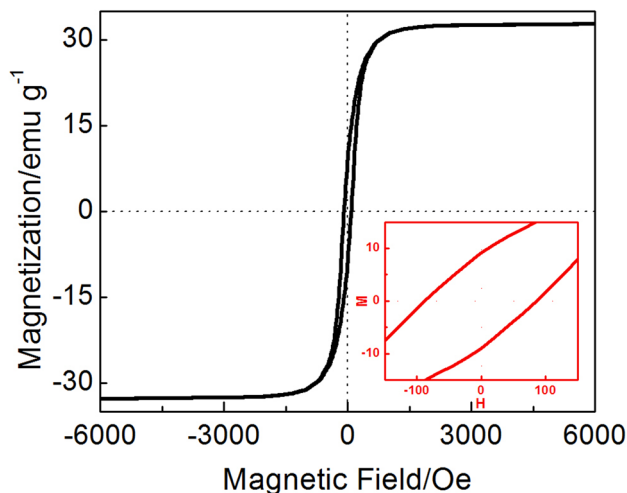


Fig. 5 Magnetic hysteresis loops of Co-P/pollen composites at room temperature with the inset of details around zero magnetic fields

Fig. 4 N₂ adsorption–desorption isotherms and pore size distribution of pollen (a) and Co-P/pollen composites (b)

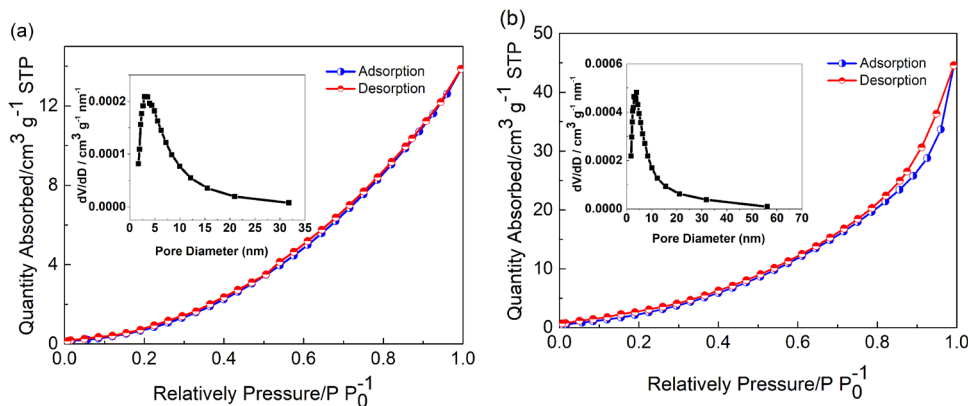


Fig. 6 Frequency dependence of complex permittivity (a) and complex permeability (b) of Co-P/pollen composites

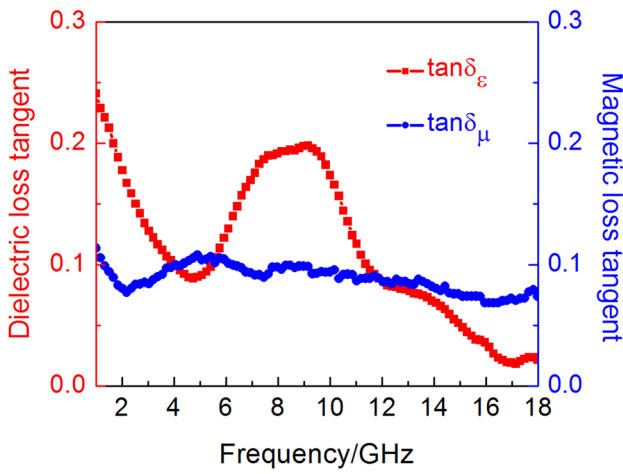
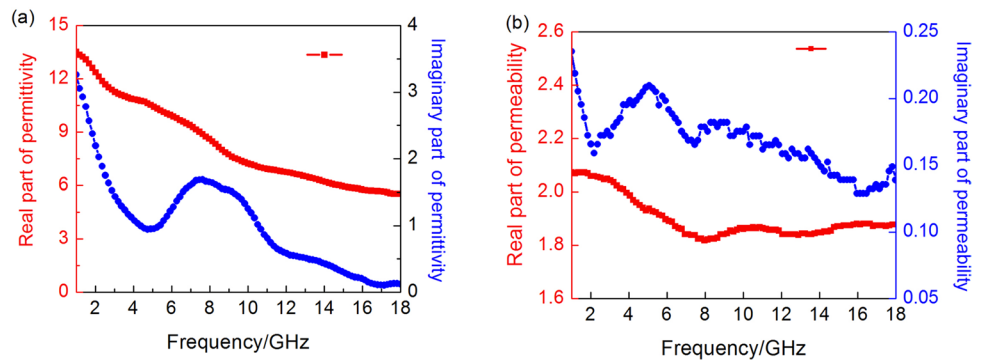


Fig. 7 Dielectric and magnetic loss tangents of Co-P/pollen composites

frequency range. In 5.0–8.2 GHz, the increased tendency of α is consistent with $\tan\delta_\epsilon$ while contrary to $\tan\delta_\mu$, indicating that dielectric loss has predominant effects in microwave attenuation of Co-P/pollen composites [30].

3.3 Microwave absorption performance

According to transmission line theory [2, 13, 28], reflection loss (RL) values as the function of frequency and thickness are calculated by the following expressions:

$$RL = 20 \log \left| \frac{Z_{in} - Z_0}{Z_{in} + Z_0} \right| \tag{3}$$

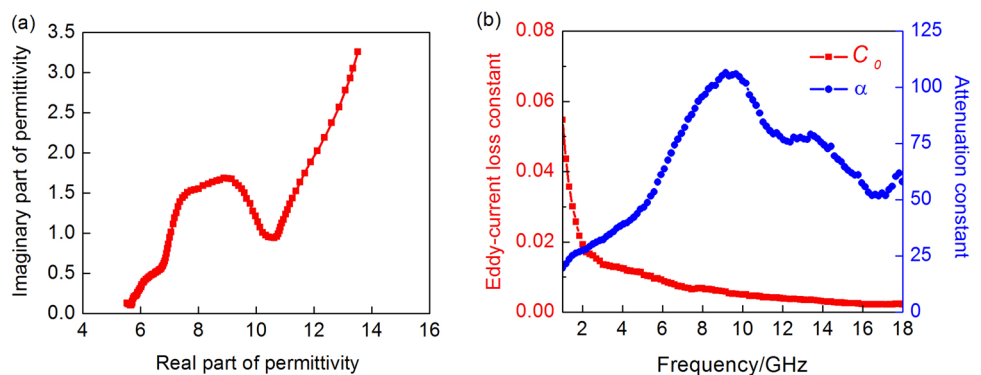
$$Z_{in} = Z_0 \sqrt{\frac{\mu_r}{\epsilon_r} \tan h \left[j \frac{2\pi f d}{c} \sqrt{\mu_r \epsilon_r} \right]} \tag{4}$$

$$\alpha = \left(\sqrt{2\pi f / c} \right) \times \sqrt{(\mu''\epsilon'' - \mu'\epsilon') + \sqrt{(\mu''\epsilon'' - \mu'\epsilon')^2 + (\mu''\epsilon' + \mu'\epsilon'')^2}} \tag{2}$$

where c is the propagation velocity of electromagnetic wave in vacuum. The attenuation constant curve displayed in Fig. 8b indicates a high value of α beyond 75 in X band (8.0–12.0 GHz), implying strong attenuation in this

where Z_{in} and Z_0 are input characteristic impedance and theoretical impedance in free space, respectively. Figure 9 presents 3D reflection loss and contour map of Co-P/pollen composites at various thicknesses and frequencies. Three

Fig. 8 Cole–Cole curves (a); eddy-current loss constant C_0 and attenuation constant α of Co-P/pollen composites



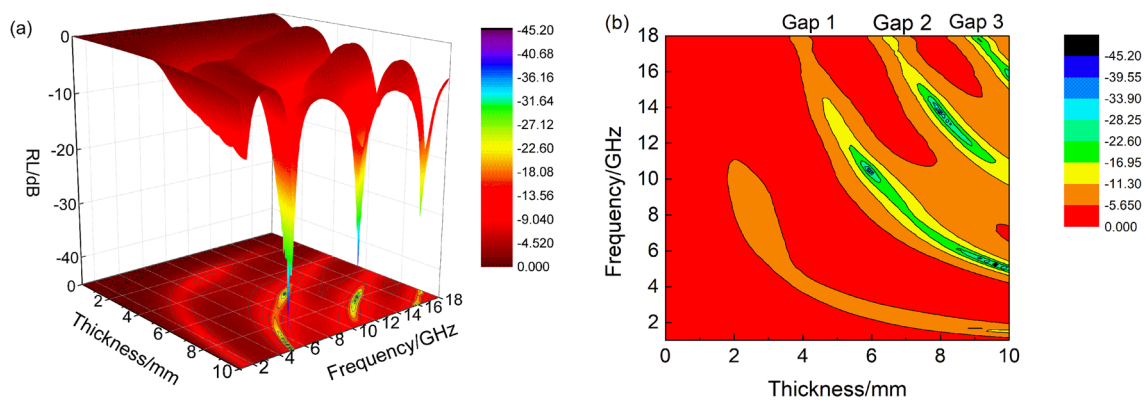


Fig. 9 3D reflection loss (a) and contour map (b) of Co-P/pollen composites at various thicknesses and frequencies

microwave absorption gaps can be seen in the RL diagram, where the minimum values of RL are shifted towards lower frequency as the thickness increases. From the gap 1 marked in Fig. 9b, the minimum RL value (RL_{\min}) reaches -41.4 dB at 13.8 GHz with the thickness of 8.0 mm. The RL_{\min} is further decreased to about -45.1 dB at the frequency of 5.3 GHz in gap 2, and the effective microwave absorption bandwidth of Co-P/pollen composites is up to 4.3 GHz. From a literature survey, RL_{\min} and effective microwave absorption bandwidth of Co-P/pollen composites are superior than those of walnut shell-derived porous carbon [31], CoNi/N-GCT [32], and CoFe₂O₄@graphene composites [33]. Consequently, electroless-plated Co-P coatings on carbonized rape pollen are proved to be an effective way to enhance microwave absorption performance, which has potential applications in electromagnetic interference shielding and attenuation.

4 Conclusions

Co-P/pollen composites were prepared by electroless plating in an alkaline solution after the rape pollen was pretreated to uncover its peculiar microporous structures. Materials characterization revealed that numerous Co-P nanoparticles with average diameters of 90 nm were distributed uniformly as coatings on and inside pollen walls. Electromagnetic analysis illustrated the typical ferromagnetism of Co-P/pollen composites with saturation magnetization of 32.6 emu g⁻¹ and coercivity of 125.1 Oe. Dielectric loss exhibited predominant effects than magnetic loss in frequency ranges of 5.0 – 8.2 GHz. An excellent microwave absorption performance was obtained, with the minimum reflection loss of -45.1 dB and the effective microwave absorption bandwidth up to 4.3 GHz.

Acknowledgements This work was supported by the Fundamental Research Funds for the Central Universities of China (No.2019ZDPY22).

Author contributions All authors have contributions in this study, either in the experimental operations or in the written of the manuscript.

Funding The present study is supported by the Fundamental Research Funds for the Central Universities of China (No.2019ZDPY22).

Availability of data and materials All the data and materials in the present study are of consistency and repeatability.

Declarations

Conflict of interest The authors declare that they have no known competing financial interests or personal relationships that could have appeared to influence the work reported in this paper.

References

- Zhang Y, Huang Y, Zhang T, Chang H, Xiao H, Chen H, Huang Z, Chen Y (2015) Broadband and tunable high-performance microwave absorption of an ultralight and highly compressible graphene foam. *Adv Mater* 27:2049–2053
- Chu W, Wang Y, Du Y, Qiang R, Tian C, Han X (2017) FeCo alloy nanoparticles supported on ordered mesoporous carbon for enhanced microwave absorption. *J Mater Sci* 52:13636–13649
- Zhao J, Liu L, Jiang R, Zhang H (2019) Dielectric relaxation and magnetic resonance in microwave absorption performance of Co_xFe_{3-x}O₄ ($0 \leq x \leq 1$) nanocrystals. *Ceram Int* 45:18347–18355
- Qiao M, Lei X, Ma Y, Tian L, He X, Su K, Zhang Q (2018) Application of yolk-shell Fe₃O₄@N-doped carbon nanochains as highly effective microwave-absorption material. *Nano Res* 11:1500–1519
- Bateer B, Zhang J, Zhang H, Zhang X, Wang C, Qi H (2018) Easily dispersible NiFe₂O₄/RGO composite for microwave absorption properties in the X-Band. *J Electron Mater* 47:292–298
- Ye W, Li W, Sun Q, Yu J, Gao Q (2018) Microwave absorption properties of lightweight and flexible carbon fiber/magnetic particle composites. *Rsc Adv* 8:24780–24786
- Wang C, Shen Y, Wang X, Zhang H, Xie A (2013) Synthesis of novel NiZn-ferrite/polyaniline nanocomposites and their

- microwave absorption properties. *Mater Sci Semicond Process* 16:77–82
8. Kumari S, Panigrahi A, Singh SK, Mohapatra M, Khanna AS, Mishra SK, Pradhan SK (2019) Electrochemical behavior of nanostructured graphene nickel phosphorus composite coating on copper. *J Appl Electrochem* 49:1157–1166
 9. Yang W, Fu Y, Xia A, Zhang K, Wu Z (2012) Microwave absorption property of Ni–Co–Fe–P-coated flake graphite prepared by electroless plating. *J Alloys Compd* 518:6–10
 10. Li Y, Wang R, Qi F, Wang C (2008) Preparation, characterization and microwave absorption properties of electroless Ni–Co–P-coated SiC powder. *Appl Surf Sci* 254:4708–4715
 11. Xiao K, Wang T, Sun M, Hanif A, Gu Q, Tian B, Jiang Z, Wang B, Sun H, Shang J, Wong PK (2020) Photocatalytic bacterial inactivation by a rape Pollen-MoS₂ biohybrid catalyst: synergetic effects and inactivation mechanisms. *Environ Sci Technol* 54:537–549
 12. Wang K, Chen Y, Tian R, Li H, Zhou Y, Duan H, Lin H (2018) Porous Co–C core–shell nanocomposites derived from Co-MOF-74 with enhanced electromagnetic wave absorption performance. *ACS Appl Mater Interfaces* 10:11333–11342
 13. Fang J, Liu T, Chen Z, Wang Y, Wei W, Yue X, Jiang Z (2016) A wormhole-like porous carbon/magnetic particles composite as an efficient broad band electromagnetic wave absorber. *Nanoscale* 8:8899–89099
 14. Lu S, Shao J, Yuan L, Wang X, Ma K, Zhang L, Meng Q (2017) Preparation and microwave-absorbing properties of hollow glass microspheres double-coated with Co-Ni/Fe₃O₄ composite. *J Mater Sci Mater Electron* 28:8878–8884
 15. Zhao H, Cheng Y, Ma J, Zhang Y, Ji G, Du Y (2018) A sustainable route from biomass cotton to construct lightweight and high-performance microwave absorber. *Chem Eng J* 339:432–441
 16. Cao F, Li D (2009) Morphology-controlled synthesis of SiO₂ hollow microspheres using pollen grain as a biotemplate. *Biomed Mater*. <https://doi.org/10.1088/1748-6041/4/2/025009>
 17. Wang L, Guan H, Hu J, Huang Q, Dong C, Qian W, Wang Y (2019) Jute-based porous biomass carbon composited by Fe₃O₄ nanoparticles as an excellent microwave absorber. *J Alloys Compd* 803:1119–1126
 18. Zhang Y, Yao Q, Zhang Y, Cui T, Li D, Liu W, Lawrence W, Zhang Z (2008) Solvothermal synthesis of magnetic chains self-assembled by flowerlike cobalt submicrospheres. *Cryst Growth Des* 8:3206–3212
 19. Zhang Y, Zhang H, Wu X, Deng Z, Zhou E, Yu Z (2019) Nanolayered cobalt@carbon hybrids derived from metal–organic frameworks for microwave absorption. *ACS Appl Nano Mater* 2:2325–2335
 20. Gómez E, Vallés E (2002) Thick cobalt coatings obtained by electrodeposition. *J Appl Electrochem* 32:693–700
 21. Goel V, Anderson P, Hall J, Robinson F, Bohm S (2016) Electroless Co–P–Carbon Nanotube composite coating to enhance magnetic properties of grain-oriented electrical steel. *J Magn Magn Mater* 407:42–45
 22. Zhang H, Chen Z, Wei X, Ou X (2017) Microwave absorbing properties of modified kaolinite coated with Co-P by electroless plating. *Rare Metal Mater Eng* 46:2244–2248
 23. Liu X, Hao C, Jiang H, Zeng M, Yu R (2017) Hierarchical NiCo₂O₄/Co₃O₄/NiO porous composite: a lightweight electromagnetic wave absorber with tunable absorbing performance. *J Mater Chem C* 5:3770–3778
 24. Wang X, Pan F, Xiang Z, Zeng Q, Pei K, Che R (2020) Magnetic vortex core-shell Fe₃O₄@C nanorings with enhanced microwave absorption performance. *Carbon* 157:130–139
 25. Song Q, Ye F, Kong L, Shen Q, Han L, Feng L, Yu G, Pan Y, Li H (2020) Graphene and MXene nanomaterials: toward high-performance electromagnetic wave absorption in gigahertz band range. *Adv Funct Mater* 30:31
 26. Liu T, Lin N, Gai L, An Q, Xiao Z, Zhai S, Cai W, Wang H, Li Z (2020) Hierarchical carbonaceous composites with dispersed Co species prepared using the inherent nanostructural platform of biomass for enhanced microwave absorption. *Microporous Mesoporous Mater* 302:110210
 27. Liu W, Liu L, Ji G, Li D, Zhang Y, Ma J, Du Y (2017) Composition design and structural characterization of MOF-derived composites with controllable electromagnetic properties. *ACS Sustain Chem Eng* 5:7961–7971
 28. Xue J, Zhang H, Zhao J, Ou X, Ling Y (2020) Characterization and microwave absorption of spinel MFe₂O₄ (M = Mg, Mn, Zn) nanoparticles prepared by a facile oxidation-precipitation process. *J Magn Magn Mater* 514:167168
 29. Liu Y, Zhang S, Su X, Xu J, Li Y (2020) Enhanced microwave absorption properties of Ti₃C₂ MXene powders decorated with Ni particles. *J Mater Sci* 55:10339–10350
 30. Zhang H, Zhao J, Ou X (2017) Facile synthesis of Fe₃O₄ nanowires at low temperature (80 °C) without autoclaves and their electromagnetic performance. *Mater Lett* 209:48–51
 31. Qiu X, Wang L, Zhu H, Guan Y, Zhang Q (2017) Lightweight and efficient microwave absorbing materials based on walnut shell-derived nano-porous carbon. *Nanoscale* 9:7408–7418
 32. Zhang X, Zhang X, Yuan H, Li K, Ouyang Q, Zhu C, Zhang S, Chen Y (2020) CoNi nanoparticles encapsulated by nitrogen-doped carbon nanotube arrays on reduced graphene oxide sheets for electromagnetic wave absorption. *Chem Eng J*. <https://doi.org/10.1016/j.cej.2019.123208>
 33. Wang S, Zhao Y, Xue H, Xie J, Feng C, Li H, Shi D, Muhammad S, Jiao Q (2018) Preparation of flower-like CoFe₂O₄@graphene composites and their microwave absorbing properties. *Mater Lett* 223:186–189

Publisher's Note Springer Nature remains neutral with regard to jurisdictional claims in published maps and institutional affiliations.